Interference Effects on (e, $2e$) Electron Momentum Profiles of CF_4

Noboru Watanabe,[1] XiangJun Chen,[2,3] and Masahiko Takahashi[1,*]

[1]*Institute of Multidisciplinary Research for Advanced Materials, Tohoku University, Sendai 980-8577, Japan*
[2]*Hefei National Laboratory for Physical Sciences at the Microscale, University of Science and Technology of China,
Hefei 230026, China*
[3]*Department of Modern Physics, University of Science and Technology of China, Hefei 230026, China*

Interference effects on electron momentum profiles have been studied using binary (e, $2e$) spectroscopy
for the three outermost molecular orbitals of CF_4, which are composed of the F $2p$ nonbonding atomic
orbitals. An analysis of the measured spherically averaged electron momentum densities has clearly
shown the presence of oscillatory structures having direct information about the internuclear distance
between the F atoms. Furthermore, it is demonstrated that the phase of the oscillatory structures depends
upon the orientation in space of the constituent atomic orbitals.

Electron momentum spectroscopy (EMS), also known as binary (e, $2e$) spectroscopy, is a kinematically complete electron-impact ionization experiment under the high-energy Bethe ridge conditions [1–3]. It is now well documented that the EMS cross section is directly related to the one-electron momentum density distribution of the ionized orbital [1–3]. Hence, one may conceive that EMS can serve as a powerful means for developing momentum-space chemistry, which was proposed in early 1940s by Coulson and Duncanson [4] and later extended by Epstein and Tanner [5]. Indeed, this is the case. The ability of EMS to probe electron momentum densities has long been displayed in terms of the inverse spatial reversal property [1–5]. Namely, since the position- (r-) and momentum-space (p-space) wave functions of any system are related by the Dirac-Fourier transform, an expansion in the r-space electronic wave function corresponds to a contraction in the p-space function. This is the material reason why EMS has proven sensitive to the behavior of outer, loosely bound electrons that are of central importance in chemical properties such as bonding, reactivity, and molecular recognition [1–3].

There is, however, another attractive property of momentum-space chemistry: bond oscillation [1–3]. Generally speaking, in the linear combination of atomic orbitals (AOs) description of a p-space molecular orbital (MO), the information about the equilibrium nuclear positions R_j is present only in the phase factors, $\exp(-i\boldsymbol{p} \cdot \boldsymbol{R}_j)$, introduced by the Dirac-Fourier transform; in p space all of the molecular structural information is contained in the interference terms arising from the phase factors. Thus the electron momentum density of a MO should exhibit, for instance, cosinusoidal or sinusoidal modulations with periodicity of $2\pi/R_{jk}$ along the direction of the line connecting atoms j and k, separated by the distance, R_{jk}. This phenomenon is called bond oscillation [5,6]. However, despite this attractive feature, to our best knowledge there

have been no EMS experiments on bond oscillation, except for the very preliminary indication noted by Leung and Brion from the EMS cross sections of CF_4 measured at binding energy of 14.7 eV [7]. This situation can be accounted for by considering experimental difficulties in conducting a high statistics EMS measurement while covering a wide momentum range so that at least one cycle of the modulation is covered.

The present Letter represents the first time that EMS cross sections are analyzed in depth to make bond oscillation visible. In addition, it is demonstrated that the phase of the oscillatory structures depends upon the orientation in space of the constituent AOs. The target molecule of this work is CF_4. This tetrahedral molecule is among the first systems to be studied for the following two reasons. First, since the three outermost MOs of CF_4 are each essentially due to lone-pair electrons or $2p$ AOs on the F atoms [7], they may give prominent oscillatory structures. Second, the large F-F internuclear distance results in the first oscillation to occur at a short momentum range that existing EMS spectrometers can cover.

EMS involves coincident detection of two outgoing electrons produced by electron-impact ionization. With the aid of energy and momentum conservation laws, the binding energy of the target electron, E_{bind}, and recoil momentum of the residual ion, $\boldsymbol{q}$, can be determined:

$$E_{bind} = E_0 - E_1 - E_2, \tag{1}$$

$$\boldsymbol{q} = \boldsymbol{p}_0 - \boldsymbol{p}_1 - \boldsymbol{p}_2. \tag{2}$$

Here, E_j's and $\boldsymbol{p}_j$'s ($j = 0, 1, 2$) are kinetic energies and momenta of the incident, inelastically scattered, and ejected electrons, respectively. Under the high-energy Bethe ridge conditions, (e, $2e$) ionization occurs due to a binary collision between the incident electron and a target electron, while the residual ion acts as a spectator. Hence the momentum of the target electron $\boldsymbol{p}$, before ionization,

is equal in magnitude and opposite in sign to the ion recoil momentum:

$$\boldsymbol{p} = -\boldsymbol{q} = \boldsymbol{p}_1 + \boldsymbol{p}_2 - \boldsymbol{p}_0. \quad (3)$$

For CF_4, two independent EMS measurements were carried out using different symmetric-noncoplanar $(e, 2e)$ spectrometers [8,9]. One was performed at $E_0 = 2.0$ keV with a low energy resolution [8] being exploited to achieve higher statistics of the experimental data. The other was conducted at a lower E_0 value of 1.6 keV with additional use of the preretardation technique for the outgoing electrons to be detected [9] to improve the energy-resolution. Note that in the symmetric-noncoplanar geometry, where two outgoing electrons having equal energies and making equal scattering angles of 45° with respect to $\boldsymbol{p}_0$ are detected, the magnitude of $\boldsymbol{p}$ can be determined from the out-of-plane azimuthal angle difference between the two outgoing electrons $(\Delta\phi)$.

Figures 1(a) and 1(b) show an example of binding energy spectra of CF_4 measured at $E_0 = 2.0$ and 1.6 keV, respectively. The spectra at $\Delta\phi = 0.5°$ are presented here. It is clear from Fig. 1(a) that since the binding energies of the three outermost $(1t_1, 4t_2,$ and $1e)$ MOs are 16.1, 17.4, and 18.5 eV respectively [7], their transition bands are inextricably overlapped owing to rather poor energy-resolution (4.9 eV fwhm) employed. This is partly because the measurement aimed to achieve high statistical precision at the expense of energy resolution. However, the
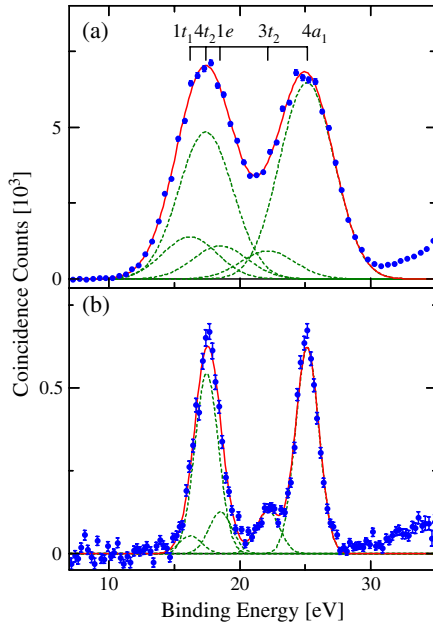
three MOs are well separated in energy from the next occupied MO, $3t_2$, at 22.2 eV. Hence electron momentum profile, which represents momentum or $\Delta\phi$-angle dependence of the EMS cross section, has been created by summing up contributions from the $1t_1$, $4t_2$, and $1e$ MOs. On the other hand, it can be seen from Fig. 1(b) that the better energy resolution (2.0 eV fwhm) achieved in the 1.6 keV measurement allows us to extract contributions from individual MOs by a curve fitting procedure. Thus momentum profiles of the $1t_1$, $4t_2$, and $1e$ MOs have been produced separately by conducting a similar fitting procedure for binding energy spectra at each $\Delta\phi$ angle $(-40° \sim 40°)$. We will discuss first the orbitally unresolved $(1t_1 + 4t_2 + 1e)$ momentum profile, and then do the orbitally resolved results.

Figure 2(a) shows the experimental $(1t_1 + 4t_2 + 1e)$ momentum profile measured at 2.0 keV. Note that the statistical precision of the present result is dramatically improved, compared with that achieved in earlier EMS studies on CF_4 [7,10]. Also included in this figure are associated theoretical momentum profiles calculated using the plane wave impulse approximation [1–3], which gives the EMS cross section for a gaseous target as

$$\sigma_{\text{EMS}}(p) = (2\pi)^4 \frac{p_1 p_2}{p_0} f_{ee} S_\alpha^f \frac{1}{4\pi} \int |\psi_\alpha(\boldsymbol{p})|^2 d\Omega_p. \quad (4)$$

FIG. 1 (color online). Binding energy spectra of CF_4 measured at an azimuthal angle difference $\Delta\phi = 0.5°$ and at $E_0 = $ (a) 2.0 and (b) 1.6 keV. Vertical bars indicate the ionization energies of the outer valence orbitals. The broken curves represent the Gaussian deconvolution functions of the data and the solid curve their sum.
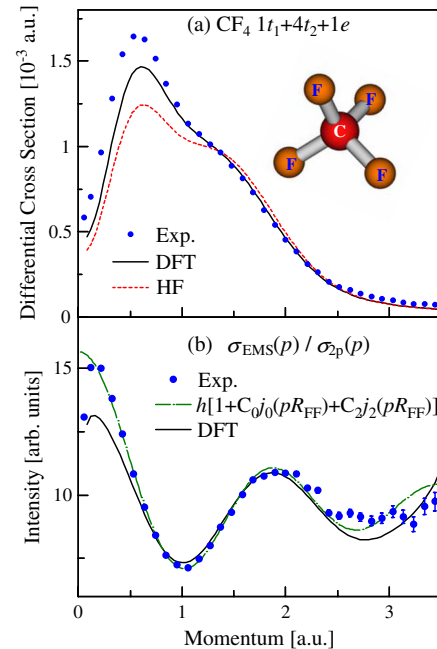

FIG. 2 (color online). (a) Comparison of experimental and theoretical momentum profiles for the sum of contributions from the three outermost molecular orbitals of CF_4 measured at $E_0 = 2.0$ keV. (b) Experimental bond oscillation for the three outermost molecular orbitals. The chain and solid lines represent results of a least-squares fit to the experiment and the associated DFT calculation, respectively.

Here, $\psi_\alpha(\boldsymbol{p})$ is the p-space representation of the normalized Dyson orbital and $S_\alpha{}^f$ is spectroscopic factor. f_{ee} is the electron-electron collision factor, which can be regarded as a constant under the present experimental conditions, and $(4\pi)^{-1}\int d\Omega_p$ represents the spherical averaging due to random orientation of gaseous molecular targets. In the calculations, $\psi_\alpha(\boldsymbol{p})$ was approximated by the corresponding Hartree-Fock (HF) or Kohn-Sham orbital [11]. Namely, the associated theoretical momentum profiles were generated by the HF method and the density functional theory (DFT) method with B3LYP functional [12], while the aug-cc-pCVTZ basis set [13] was used. Briefly, $1t_1$, $4t_2$, and $1e$ MO wave functions were generated in r space by the GAUSSIAN98 program [14] and they were subsequently converted to momentum profiles with the aid of the HEMS program developed by Brion and others [15]. The resulting momentum profiles have been folded with the instrumental momentum resolution (for instance, 0.21 a.u. at $p \approx 1$ a.u. in the 2.0 keV measurement), and the theoretical $(1t_1 + 4t_2 + 1e)$ momentum profile has been created by summing up those, assuming the spectroscopic factor value of unity for each orbital. To make a comparison between the experiment and theory, the experimental result has been height-normalized to the theoretical prediction at $p = 1.36$ a.u., where the HF and DFT calculations give the same intensity.

It can be seen from Fig. 2(a) that the HF calculation substantially underestimates the experimental intensity in the low momentum region, $p < \sim 1.3$ a.u. The difference in intensity is considerably reduced by the DFT calculation, indicating noticeable electron correlation effects in the three outermost orbitals. Also can be seen from Fig. 2(a) is that the experiment shows a shoulder at $p \approx 1.4$ a.u., which is analogous to the shoulder that was observed and assigned by Leung and Brion [7] as an indication of bond oscillation. Nevertheless, we can now present conclusive evidence of bond oscillation through the following analysis.

Since the $1t_1$, $4t_2$, and $1e$ MOs consist of the F $2p$ AOs, they each can be described as

$$\psi_\alpha(\boldsymbol{r}) = \sum_{j=1}^{4} c_j \chi_{2p}(r_j)\left[\sum_{m=-1}^{1} a_{j,m} Y_{1,m}(\hat{r}_j)\right]. \quad (5)$$

Here, c_j's are coefficients of the linear combination of AOs expansion, $\chi_{2p}(r_j)$ is the radial part of the F $2p$ AO centered at the jth F atom position $\boldsymbol{R}_j$, and $r_j = \boldsymbol{r} - \boldsymbol{R}_j$. $Y_{1,m}$ denotes spherical harmonics with the total angular momentum quantum number of $\ell = 1$ and magnetic quantum number of m. Spatial orientation, in the molecular frame, of the jth $2p$ AO is defined by a set of coefficients $a_{j,m}$'s, which satisfy $|a_{j,-1}|^2 + |a_{j,0}|^2 + |a_{j,1}|^2 = 1$. The Dirac-Fourier transform is then performed to generate the p-space representations of the MOs:

$$\psi_\alpha(\boldsymbol{p}) = \chi_{2p}(p)\sum_{j=1}^{4} c_j \exp(i\boldsymbol{p}\cdot\boldsymbol{R}_j)\sum_{m=-1}^{1} a_{j,m} Y_{1,m}(\hat{\boldsymbol{p}}), \quad (6)$$

with

$$\chi_{2p}(p) = i\sqrt{\frac{2}{\pi}}\int j_1(pr)\chi_{2p}(r)r^2 dr. \quad (7)$$

Here $j_n(pr)$ is the spherical Bessel function of order n. From Eqs. (4) and (6) we have

$$\sigma_{EMS}(p) = \sigma_{2p}(p)\, S_\alpha^f \sum_{j,k} c_j c_k \int \exp(i\boldsymbol{p}\cdot\boldsymbol{R}_{jk})$$
$$\times\left[\sum_{m,m'} a_{j,m} a_{k,m'}^* Y_{1,m}(\hat{\boldsymbol{p}})Y_{1,m'}^*(\hat{\boldsymbol{p}})\right]d\Omega_{\boldsymbol{p}}, \quad (8)$$

where $\boldsymbol{R}_{jk} = \boldsymbol{R}_j - \boldsymbol{R}_k$ and $\sigma_{2p}(p) = 4\pi^3(p_1 p_2/p_0)f_{ee}|\chi_{2p}(p)|^2$, which corresponds to the EMS cross section for the $2p$ AO of an isolated F atom. Furthermore, use of identities of spherical harmonics that $\exp(i\boldsymbol{p}\cdot\boldsymbol{R}_{jk})$ can be expanded in terms of spherical harmonics [6] and that $Y_{1,m}Y_{1,m'}^*$ can be replaced with a linear combination of $Y_{0,0}$ and $Y_{2,m+m'}$ yields

$$\sigma_{EMS}(p) = \sigma_{2p}(p)S_\alpha^f h\left[1 + C_0 j_0(pR_{FF}) + C_2 j_2(pR_{FF})\right]. \quad (9)$$

Here, $h = \Sigma_j c_j^2$ and R_{FF} $(= |\boldsymbol{R}_{jk}|$ with $k \neq j)$ is the internuclear distance between the F atoms. C_0 and C_2, coefficients of the spherical Bessel functions of order 0 and 2, are given by

$$C_0 = 2\sum_{j>k} c_j c_k \cos\theta_{jk}\Big/\sum_j c_j^2, \quad (10)$$

$$C_2 = 2\sum_{j>k} c_j c_k\left[\cos\theta_{jk} - 3(\hat{\boldsymbol{\mu}}_j\cdot\hat{\boldsymbol{R}}_{jk})(\hat{\boldsymbol{\mu}}_k\cdot\hat{\boldsymbol{R}}_{jk})\right]\Big/\sum_j c_j^2, \quad (11)$$

where θ_{jk} is the angle between the orientations of the constituent $2p$ AOs located on F atoms j and k. $\hat{\boldsymbol{\mu}}_j$ and $\hat{\boldsymbol{\mu}}_k$ are unit vectors codirectional with the orientations of the $2p$ AOs and $\hat{\boldsymbol{R}}_{jk} = \boldsymbol{R}_{jk}/|\boldsymbol{R}_{jk}|$. Note that the coefficients C_0 and C_2 take constant values for each MO. In this way the function $h[1 + C_0 j_0(pR_{FF}) + C_2 j_2(pR_{FF})]$ governs the oscillatory behavior, so it is henceforth referred to as the interference factor.

In order to examine the role of the interference factor, we present in Fig. 2(b) the experimental $(1t_1 + 4t_2 + 1e)$ result in the form of its momentum profile divided by $\sigma_{2p}(p)$. Here, to take into account distorted wave effects that may arise especially in the high momentum region, $\sigma_{2p}(p)$ was calculated with the distorted wave Born approximation [16] using the HF wave function reported by Clementi and Roetti [17]. It is immediately clear that the

experiment exhibits an oscillatory structure. To highlight it more closely, the function $h[1 + C_0 j_0(pR_{FF}) + C_2 j_2(pR_{FF})]$ was subsequently employed as a fitting curve to reproduce the experiment with R_{FF}, h, C_0, and C_2 being used as fitting parameters. The best fit to the experiment (chain line) is also presented in Fig. 2(b). The resulting R_{FF} value of 4.02 Bohr has been found to be in excellent agreement with 4.07 Bohr reported by electron diffraction [18]. Furthermore, the experiment is in accordance with an associated DFT calculation, shown by the solid line. The presence of bond oscillation has thus been unambiguously identified.

Next, we discuss MO-specific bond oscillation with Fig. 3, where the orbitally-resolved $1t_1$, $4t_2$, and $1e$ results, measured at 1.6 keV, are presented in the form of their momentum profiles divided by $\sigma_{2p}(p)$. Also included in Fig. 3 are the associated DFT calculations and the theoretical electron density distributions in r space. A glance at Fig. 3 shows that although the statistics of the data leaves much to be desired, the phase of the experimental oscillatory structure is largely dependent upon the MO. For instance, the $4t_2$ result shows a maximum at $p = 0$, while the $1t_1$ and $1e$ results display a minimum. These observations are supported by the DFT calculations.

The clue for understanding these observations lies, indeed, in the interference factor; the coefficients C_0 and C_2 in Eq. (9) largely depend upon the MO pattern in interest.

In particular, C_0 governs the intensities of the oscillatory structures at $p = 0$, because $j_0(0) = 1$ and $j_2(0) = 0$. Furthermore, since the constituent AOs considered here are equivalent, c_j's for each MO, the coefficients of the linear combination of AOs expansion in Eq. (5), have the same value. As a result, the expression of C_0 given by Eq. (10) can be simplified to $C_0 = 1/2 \ \Sigma_{j>k} \cos\theta_{jk}$. Thus, by keeping in mind that the $4t_2$ MO is a triply degenerate orbital, the maximum intensity value of c.a. 12 at $p = 0$ means that the constituent $2p$ AOs are completely oriented in the same direction. On the other hand, for the $1t_1$ and $1e$ MOs, the $2p$ AOs are oriented so that the interference factor value tends to zero at $p = 0$. These findings are consistent with the theoretical electron density distributions.

In short, the measured electron momentum profiles for the three outermost MOs of CF_4 have successfully been employed to demonstrate, for the first time, the presence of bond oscillation in EMS cross sections. Further, it has been shown that the phase of the oscillatory structures depends upon the orientation in space of the constituent AOs. We expect that future efforts will be dedicated along this line to various molecular targets, to enrich momentum-space chemistry. For this purpose extensive use of the latest version of EMS spectrometers [19,20] would be desired, which have produced considerable improvement in instrumental sensitivity and extended the coverable momentum range by a factor of about 3 compared with the EMS spectrometers employed here.
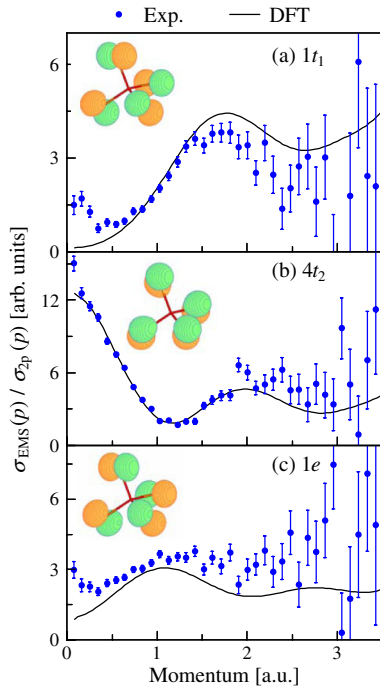
FIG. 3 (color online). Comparison of experimental and DFT bond oscillations for the (a) $1t_1$, (b) $4t_2$, and (c) $1e$ molecular orbitals of CF_4 measured at $E_0 = 1.6$ keV. The inserted figures are the corresponding theoretical electron density distributions in r space.

*Author to whom correspondence should be addressed.
masahiko@tagen.tohoku.ac.jp

[1] E. Weigold and I. E. McCarthy, *Electron Momentum Spectroscopy* (Kluwer Academic/Plenum Publishers, New York, 1999).

[2] M. A. Coplan, J. H. Moore, and J. P. Doering, Rev. Mod. Phys. **66**, 985 (1994).

[3] M. Takahashi, Bull. Chem. Soc. Jpn. **82**, 751 (2009).

[4] For instance, C. A. Coulson, Proc. Cambridge Philos. Soc. **37**, 55 (1941); C. A. Coulson and W. E. Duncanson, *ibid.* **37**, 67 (1941).

[5] I. R. Epstein and A. C. Tanner, in *Compton Scattering*, edited by B. G. Williams (McGraw-Hill, New York, 1997).

[6] J. P. D. Cook and C. E. Brion, Chem. Phys. **69**, 339 (1982).

[7] K. T. Leung and C. E. Brion, Chem. Phys. **91**, 43 (1984).

[8] M. Takahashi, N. Watanabe, Y. Khajuria, K. Nakayama, Y. Udagawa, and J. H. D. Eland, J. Electron Spectrosc. Relat. Phenom. **141**, 83 (2004).

[9] M. Takahashi, T. Saito, M. Matsuo, and Y. Udagawa, Rev. Sci. Instrum. **73**, 2242 (2002).

[10] R. Cambi, G. Ciullo, A. Sgamellotti, F. Tarantelli, R. Fantoni, A. Giadini-Guidoni, M. Rosi, and R. Tiribelli, Chem. Phys. Lett. **90**, 445 (1982).

[11] P. Duffy, D. P. Chong, M. E. Casida, and D. R. Salahub, Phys. Rev. A **50**, 4707 (1994).

[12] A. D. Becke, J. Chem. Phys. **98**, 5648 (1993).

[13] T. H. Dunning, Jr., J. Chem. Phys. **90**, 1007 (1989).

[14] M. J. Frisch *et al.*, GAUSSIAN98, *Revision A.7* (Gaussian, Inc., Pittsburgh PA, 1998).

[15] A. O. Bawagan, C. E. Brion, E. R. Davidson, and D. Feller, Chem. Phys. **113**, 19 (1987).

[16] I. E. McCarthy, Aust. J. Phys. **48**, 1 (1995).

[17] E. Clementi and C. Roetti, At. Data Nucl. Data Tables **14**, 177 (1974).

[18] M. Fink, C. W. Schmiedekamp, and D. Gregory, J. Chem. Phys. **71**, 5238 (1979).

[19] M. Yamazaki, H. Satoh, M. Ueda, D. B. Jones, Y. Asano, N. Watanabe, A. Czasch, O. Jagutzki, and M. Takahashi, Meas. Sci. Technol. **22**, 075602 (2011).

[20] Q. G. Tian, K. D. Wang, X. Shan, and X. J. Chen, Rev. Sci. Instrum. **82**, 033110 (2011).